University Library

MINERVA ACCESS

A gateway to Melbourne's research publications

Minerva Access is the Institutional Repository of The University of Melbourne

Author/s:
Truong, SCH;Huang, Y;Siems, S;Manton, M;Lang, F

Title:
Biases in the thermodynamic structure over the Southern Ocean in ERA5 and their radiative implications

Date:
2022-04-18

Citation:
Truong, S. C. H., Huang, Y., Siems, S., Manton, M. & Lang, F. (2022). Biases in the thermodynamic structure over the Southern Ocean in ERA5 and their radiative implications. International Journal of Climatology, 42 (15), pp.7685-7702. https://doi.org/10.1002/joc.7672.

Persistent Link:
https://hdl.handle.net/11343/301576

License:
CC BY-NC-ND

Lang Francisco (Orcid ID: 0000-0002-8595-4836)
Truong Son Cong Hoang (Orcid ID: 0000-0001-6498-5214)

Biases in the thermodynamic structure over the Southern Ocean in ERA5 and their radiative implications

S. C. H. Truong[1,3], Y. Huang[2,3], S. T. Siems[1,3], M. J. Manton[1] and F. Lang[1]

[1]Monash University, Melbourne, Australia.

[2]The University of Melbourne, Melbourne, Australia.

[3]Australian Research Council Centre of Excellence for Climate Extremes (CLEX), Melbourne, Australia.

Corresponding author: Son Truong (son.truong@monash.edu)

Key Points:

- The ERA5 reanalysis under-represents the number of inferred cloud layers at high latitudes over the Southern Ocean
- Cloud layers inferred from the ERA5 profiles are geometrically thinner and shallower than those inferred from the observed soundings
- A fine-resolution representation of thin multiple cloud layers can help reduce the shortwave radiation bias over the Southern Ocean

This article has been accepted for publication and undergone full peer review but has not been through the copyediting, typesetting, pagination and proofreading process which may lead to differences between this version and the Version of Record. Please cite this article as doi: 10.1002/joc.7672

This article is protected by copyright. All rights reserved.

Accepted Article

Accepted Article

Abstract

The thermodynamic structure of the lower troposphere in the 37 standard levels ERA5 reanalysis has been evaluated against 2186 high-resolution upper air soundings collected over the Southern Ocean (SO). The reanalysis, which incorporated these soundings, was found to be skilled in depicting the general synoptic meteorology and thermodynamic structure as defined by the cluster analysis of Truong et al. (2020). Using dewpoint depression as a proxy for cloud, however, we found a significant reduction in the number of inferred cloud layers, which is inherited from a bias in the specific humidity in the ERA5 reanalysis, most notably over the high latitudes of the SO, where a multi-layer cloud structure is frequently observed. The reanalysis was also found to have thinner inferred cloud geometric layer and shallower cloud top heights. Further analysis showed that the reanalysis displays a greater percentage of soundings having no inversion with this bias being more pronounced at high latitudes that tends to be associated with the colder sea surface temperature. While the statistics of the main inversion height are largely consistent, the average inversion strength in the ERA5 reanalysis is found to be weaker than the observations. We anticipate the 137-level ERA5 reanalysis simulation yields a smoothed vertical structure, from which the 37 standard levels ERA5 reanalysis is linearly interpolated. An examination of the sensitivity of the radiative transfer to cloud macrophysics suggests that the correct representation of thin multiple cloud layers can help reduce the amount of downward shortwave surface radiation over the SO.

1. Introduction

Reanalyses are essential tools for understanding atmospheric and climate processes over the Southern Ocean (SO) because of the scarcity of in-situ observations, a consequence of the harsh and remote conditions. Precipitation variations (Manton et al., 2020), atmospheric circulation (McKay et al., 2020), and cloud macrophysics (Kuma et al., 2020) are all recent examples of SO studies dependent on reanalyses products. Despite their functionality, many past studies have also documented potential biases (e.g., cloud cover) in the reanalyses (e.g., Trenberth and Fasullo 2010; Naud et al., 2014; Klekociuk et al., 2019), particularly over the SO. While these products are subject to numerous sources of error (e.g., assimilation methods, parameterization schemes, poor observations), the lack of in-situ observations, particularly for the marine atmospheric boundary layer (MABL) where satellite observations may have limited skill (Huang et al. 2012), may be a leading source over the SO. Lang et al. (2018) reported that

the height of the main inversion diagnosed from the European Centre for Medium-Range Weather Forecasts Re-Analysis (ERA-Interim) was systematically lower in the cold sector of mid-latitude cyclones compared to the atmospheric soundings over Macquarie Island (54.61°S, 158.87°E) from 1995 to 2010. Similar biases in the thermodynamic structure of the lower troposphere were also reported both regionally and globally (e.g., Williams et al. 2013; Guo et al., 2021).

A further related challenge for reanalyses over the SO is, potentially, the common presence of a thin multilayer cloud structure that appears both within and beyond the MABL [e.g., Truong et al., 2020 (hereafter T20); Chubb et al., 2016; Mace et al., 2009; Mace and Protat 2018a]. A correct representation of a multilayer cloud structure is of scientific importance since it can have a substantial influence on the radiation budget and local heating compared to that of a single cloud layer (Li et al., 2011; 2015). A global climatology of multilayer cloud structure (Mace et al., 2009) illustrates the difference between the Northern and Southern Hemispheres, with the frequent presence of a multilayer cloud structure evident over the high latitudes of the SO. The greatest frequency of multilayer clouds can be seen to be roughly spatially correlated with the surface radiation bias (Trenberth and Fasullo, 2010).

Atlas et al. (2020) evaluated large-eddy simulations (LES) of the SO MABL in which the simulations were either forced by the ERA5 reanalysis (Hersbach et al., 2020) or aircraft dropsonde observations from the **S**outhern **O**cean **C**louds, **R**adiation and **A**erosol **T**ransport **E**xperimental **S**tudies (SOCRATES) field campaign (McFarquhar et al. 2021). They reported that ERA5-forced LES simulations failed to produce a two-layer stratus cloud structure observed in a stable MABL since these thin cloud layers were not well represented in ERA5's 37 vertical levels which was interpolated from 137 hybrid sigma/pressure levels. They further reported that ERA5 had large temperature and humidity biases around low-altitude temperature inversions due, at least in part, to inadequate vertical resolution. This highlights the challenges of using ERA5 as an initial and boundary conditions for model simulations, particularly over the SO and Antarctic regions (Huang et al., 2015; Lang et al., 2021; Vignon et al., 2021) where multi-layer mixed-phase cloud is commonly present (Mace et al., 2009).

Recently, T20 analyzed 2186 atmospheric soundings collected from the four coordinated field campaigns over the SO as detailed in McFarquhar et al. (2021) to better define the synoptic

Accepted Article

meteorology and associated structure across the MABL and lower free troposphere. Specifically, T20 used a simple k-means cluster algorithm to define seven distinct synoptic clusters across the SO sampled by the field campaigns. They observed that a multi-layer cloud structure was commonly present in the vicinity of fronts and cyclones with many clouds being as thin as 200 m and less. Motivated by T20, we extend our attention to an evaluation of the thermodynamic structure of the lower troposphere presented by ERA5. ERA5 was produced using 4DVar data assimilation in CY41R2 of ECMWF's Integrated Forecast System (IFS), operational since 2016. As noted in Atlas et al. (2020), these 2186 soundings were incorporated into the production of ERA5, yet systemic differences persist, for instance, specific humidity (Graham et al., 2019; Seethala., 2021). Sato et al. (2018) evaluated the importance of ingesting SO radiosonde observations into the generation of a reanalysis, reporting improved skills most notably at upper levels. Wang et al. (2020) reported that ERA5 showed positive biases in the shortwave radiation effects over the SO with the mean surface cloud radiative effect (CRE) being -101 W m^{-2}, whereas the observed mean surface CRE was -164 ± 100 Wm^{-2}. The authors also found that a key reason for the overestimation in ERA5 is the lower cloud fraction.

The objectives of this study are two-fold. First, we evaluate the low-level thermodynamic structure, including inferred cloud layers and inversion in the 37 standard levels ERA5 product against the aforementioned 2186 upper air soundings according to the synoptic classes identified in T20. We are interested in examining the inferred cloud macrophysics (e.g., cloud layer, cloud top height) over the SO, independent of the cloud microphysics. As significant differences arise simply due to the vertical resolution, we analyze the soundings both at 20 m resolution and the 37 standard levels (interpolated from 137 model levels) set in ERA5. Second, we examine representative soundings in detail to better quantify the sensitivity of the radiative transfer to cloud macrophysics inferred from the soundings, as per T20. For this task, we use the NASA Langley Fu-Liou radiative transfer model (RTM, Fu and Liou, 1992, 1993, 1997). A more complete description of the RTM is detailed in section 2.2.3.

This manuscript is presented as follows. Section 2 contains a description of the data and methodology. Section 3 presents the main results and evaluation of the ERA5 reanalysis, including inferred clouds and inversions. Discussion of the radiative transfer sensitivity to cloud macrophysics is in section 4, and conclusions are in section 5.

Accepted Article

Accepted Article

2. Data, Methodology and Validation

2.1. Data

2.1.1. Field observation

The 2186 atmospheric soundings were measured over a period of 28 months (January 2016 to April 2018) from four field campaigns (McFarquhar et al., 2021) as follows:

- the Clouds, Aerosols, Precipitation, Radiation, and Atmospheric Composition over the SO (CAPRICORN 2016, March–April 2016), and CAPRICORN 2018 (January–February 2018),
- the SO Clouds Radiation Aerosol Transport Experimental Study (SOCRATES, January–February 2018),
- the Measurements of Aerosols, Radiation, and Clouds over the SO Science Plan (MARCUS, October 2017 to March 2018),
- the Macquarie Island Cloud and Radiation Experiment (MICRE/ACRE, April 2016 to April 2018).

More information on the soundings (e.g., radiosonde type, level of precision and platforms) can be found at the Sub-Table 1.

2.1.2. Reanalysis

The ERA5 reanalysis (ERA5), produced by the European Centre for Medium-Range Weather Forecasts (ECMWF), is based on the global Numerical Weather Prediction (NWP) model Integrated Forecast System (IFS) version CY41R2 (Hersbach et al., 2020). The model provides hourly estimates of atmospheric variables, at a horizontal resolution of 31 km and 137 vertical levels from the surface to 0.01 hPa, presently extending back to 1950. In this analysis, we use the hourly data on the temperature, specific humidity, zonal wind [u], and meridional wind [v], pressure and surface variables (pressure, air temperature, and relative humidity). These variables are interpolated onto a horizontal grid of 0.25° × 0.25° and 37 pressure levels from its native 137 hybrid sigma/pressure levels and 31 km horizontal grid.

Accepted Article

2.1.3. Satellite-based datasets

The Clouds and the Earth's Radiant Energy System (CERES) dataset provides satellite-based observations of Earth's radiation budget (ERB) and clouds (Wielicki et al. 1996). The CERES instruments, currently onboard four satellites (i.e., Terra, Aqua, S-NPP, NOAA-20), measure broadband radiances in the shortwave (SW; 0.3-5 μm), total (0.3-200 μm) and the longwave (LW; 5-35 μm). An overview of CERES is documented at "https://ceres.larc.nasa.gov". In this study, we use the CERES_SYN1deg_Ed4.1 1Hour product (Doelling et al., 2016), which is a Level 3 product containing 1°x1° (latitude by longitude), hourly averaged observed top-of-atmosphere (TOA) radiative fluxes along with computed TOA and surface fluxes and fluxes at four atmospheric pressure levels (70, 200, 500, and 850 hPa). The CERES_1h product also contains coincident MODIS-derived cloud and aerosol properties and hourly geostationary satellite (GEO) derived cloud properties. An in-depth overview of cloud property retrievals and their uncertainty are provided in Minnis et al., (2021). In this study, we used ice/water particle effective radius as input parameters for the RTM discussed in 2.2.3.

2.2. Methodology

2.2.1. Cluster characteristics

In T20 the 2186 radiosondes were sorted into 7 clusters according to a *k*-means algorithm using 15 thermodynamic observations (the temperature, relative humidity, zonal wind, and meridional wind at the 925, 850, and 700 hPa levels and the surface pressure, air temperature, and relative humidity). In short, one warm water cluster (W1), four unique storm track clusters (M1-M4) and two cold high-latitude clusters (C1 & C2) were identified (Table 1). A comprehensive analysis of the characteristics of each cluster is presented in T20. As is a common practice, the nearest spatial and temporal ERA5 profile is matched to each of the radiosondes and placed in the corresponding cluster (e.g., Graham et al., 2019; Sato et al., 2020; Seethala., 2021).

Table 1. Summary of the thermodynamic characteristics for the seven clusters from W1 to C2 derived in T20.

Cluster	Acronym	Characteristics
warm cluster	W1	poleward warm air advection far ahead of a cold front

high-pressure cluster	M1	weak winds, a strong inversion and low relative humidity in the free troposphere; located near anticyclones and ridges
cold front cluster	M2	westerly winds with a high humidity; frequently observed in the immediate neighbourhood of a cold front.
postfrontal cluster	M3	winds from the southwest, the cold surface air temperature; commonly located behind cold front.
warm front cluster	M4	strong northwesterly winds, a weak inversion and a high relative humidity; commonly appears ahead of the cold front, consistent with the location of the warm front.
high latitude cluster	C1	weak winds, high relative humidity through the lower free troposphere; predominantly located poleward of the ocean polar front
Antarctic coastline	C2	commonly displays dry offshore flow, consistent with katabatic winds across the lowest 200–500 m

2.2.2. Cloud and inversion identification

We compare the physical characteristics of the observed atmospheric soundings and ERA5 profiles focusing on the low-level thermodynamic structure (e.g., cloud layer, inversion strength and height). We defined profiles at different resolutions as below:

- "FINE" observed profiles: the high-resolution observations were first averaged to a 20 m vertical resolution before being smoothed by a five-point filter as in T20.
- "COARSE" observed profiles: FINE was first linearly interpolated to 137 ERA5 pressure levels (see Appendix for detailed calculation). The intermediate 137 level profiles were then linearly interpolated to 37 ERA5 standard pressure levels.
- "ERA5" profiles: ERA5 from 37 ERA5 pressure levels. Note that we found no differences when comparing 37 ERA5 pressure levels and 37 ERA5 interpolated from 137 ERA5 pressure levels.

To maintain the main features of the observed sounding profiles (e.g., inversion layers/strength), interpolation was found to be better than averaging to the 37 pressure levels (Hande et al., 2012, Lang et al., 2018, Graham et al., 2019). We will more fully discuss the sensitivity of our findings to the interpolation and averaging methods in section 3.3.

For each sounding we define an inferred cloud layer by proxy as a layer with a dew point depression (i.e., the temperature and dew point temperature difference) of less than 1.5°C. Determining cloud vertical structures from the thermodynamic profiles (e.g., radiosonde) has

Accepted Article

been widely used in literature (Costa-Suros et al. 2014). According to T20, the threshold was chosen upon visual inspection. Our findings are not qualitatively sensitive to small changes (e.g., ±0.3°C) in this value. At FINE resolution, we follow T20 and require at least three consecutive layers (60 m) to reach this threshold to define a cloud layer. At COARSE resolution, only a single layer reaching this dew-point depression threshold is required to define a cloud layer. For a consistent comparison, inferred cloud layers in ERA5 soundings are also defined by the dewpoint depression, rather than using the immediate ERA5 derived cloud fields. The dew point temperature in ERA5 was calculated from the specific humidity (Bolton 1980). For each profile, the number of inferred cloud layers from 950 to 600 hPa is counted. The results are not qualitatively sensitive to these thresholds, although we note that the specified thresholds yield results consistent with Mace et al., 2009. The number of cloud layers are named "one", "two", "three", "four" and "all" to represent one-, two-, three-, four- and all-(inferred) cloud layers, respectively. No distinction is made for layers at the 950 and 600 hPa boundaries. Please note that ERA5 cloud product is modelled output spun up from an earlier time step; it is not the direct product of assimilating observation of cloud properties, both macro- and microphysics. As such, ERA5 cloud fields are subject to uncertainties that can arise from the various parameterization schemes and settings employed. Most importantly, since ERA5 cloud product is initialised at an earlier time, it is independent of the assimilated thermodynamic structure. Accordingly, we limit our analysis to the inferred cloud layer from soundings and ERA5 for a direct comparison as discussed in Costa-Surós et al. (2014).

Again following T20, we define the main inversion as the level with maximum gradient of virtual potential temperature, $d\theta_V/dp$, from 950 to 600 hPa with a minimum threshold of 0.08 K hPa^{-1}. If this threshold is not met between these levels, then "no" inversion is recorded. By this definition, we can simply count the number of inversions (i.e., $d\theta_V/dp \geq 0.08$ K hPa^{-1}) evident between 950 to 600 hPa. Again, the results are not qualitatively sensitive to these thresholds.

2.2.3. Radiative transfer model

The RTM scheme, developed by Fu and Liou (1993), is a delta-four-stream approximation. The nongray absorption of gases such as O_3, CO_2, CH_4, N_2O and H_2O is considered in the multiple-scattering inhomogeneous atmosphere using the correlated *k*-

Accepted Article

distribution method. By default, CO_2, CH_4, and N_2O are assumed to be well-mixed throughout the atmosphere with concentrations of 360, 1.6 and 0.28 ppmv, respectively. The RTM inputs include, but are not limited to, visible cloud optical depth, phase, particle size, cloud top and base heights, solar zenith angle, total solar flux, and the surface emissivity. We used the RTM to quantify the sensitivity of the radiative transfer to cloud macrophysics (e.g., the number of cloud layers, cloud height, cloud thickness). Other parameters such as the cloud microphysics (e.g., ice/water cloud effective diameter/radius) are taken from the CERES dataset.

We present two case studies from representative atmospheric profiles. The profile provides the pressure, temperature, water vapor, ozone concentration (acquired from ERA5) profiles as model inputs to calculate the SW and LW fluxes through the atmosphere. These fluxes are used to quantify the impacts of vertical resolution on the radiation at the surface and the top of the atmosphere. The optical depth is estimated following Bennartz (2007) and Huang et al., (2016) as:

$$\tau = \frac{9}{10} c_w \times D^2 \times \frac{1}{r_{eff}} \times \frac{1}{\rho_l}, \qquad (1)$$

Where τ is the cloud optical depth, r_{eff} is the effective radius (μm) taken from CERES data, ρ_l is liquid water density (1.0×10^3 kg m^{-3}), c_w is the temperature-dependent condensation rate (g m^{-4}). As per Huang et al., (2016), c_w was set to 80% of adiabaticity with a lower temperature range at 233 K and D is the cloud layer thickness.

The detailed RTM's inputs are listed in Table S1 in the supporting document.

3. ERA5 evaluation

3.1. Mean profile

Overall, the cluster-average ERA5 profiles are very comparable to those from the observations (Fig. 2), suggesting that ERA5 strongly captures the distinct low-level thermodynamic structures over the SO. The temperature profiles are consistent between the two datasets, although small discrepancies are noted in the lower troposphere (0.1°C). This agreement is not particularly surprising, given that these soundings were employed in producing ERA5. While the dewpoint temperature profiles demonstrate a high degree of agreement between the observed and ERA5 (e.g., M3, C1), it also suggests that a slightly dry/wet (0.5-1°C)

Accepted Article

bias exists in the lower/upper parts of the atmosphere, particularly in the post-frontal cluster M3, although these differences are not statistically significant at the 95% confidence level according to the Student's *t*-test. These differences may be associated with (i) the tempo-spatial discrepancies between ERA5 and sounding observations and (ii) biases in the specific humidity in ERA5 which is used to calculate the dewpoint.

A comparison of mean profiles between 137 and 37 ERA5 pressure levels shows that 37 ERA5 pressure levels were superimposed on 137 ERA5 pressure levels. In other word, the difference between the 37 ERA5 pressure levels interpolated from 137 ERA5 pressure levels and 37 ERA5 pressure levels directly downloaded is insignificant (<0.05°C) over the range of 950 – 600 hPa. Using either 137 or 37 ERA5 pressure levels has no significant impact on either the number of inferred cloud layers or the radiation calculation in section 3.3 and 4, respectively.

Table 2. Comparison of ERA5's and observations' characteristics presented in thermodynamics, COARSE inversion statistics and statistical metrics, for the seven clusters from W1 to C2. The numbers in INV macrophysics and cloud statistics present the mean and one standard deviation. The differences in cloud statistics between the COARSE and ERA5 are statistically significant at the 95% confidence level, indicated by bold numbers.

Name of cluster	W1	M1	M2	M3	M4	C1	C2
Total count	209	272	507	407	334	318	139
I. Main inversion (INV) statistic							
a) no INV (%)							
COARSE	4.3	5.2	29.4	21.4	37.4	33.3	8.6
ERA5	10.5	9.6	38.9	33.2	55.4	55.7	25.9
b) INV macrophysics							
COARSE							
INV height (hPa)	860.0 ± 78.4	863.0 ± 72.6	782.7 ± 101.0	775.7 ± 81.7	833.1 ± 104.0	799.1 ± 95.7	792.2 ± 80.8
INV strength (K.hPa^{-1})	0.18 ± 0.08	0.18 ± 0.07	0.14 ± 0.04	0.15 ± 0.05	0.13 ± 0.05	0.14 ± 0.04	0.14 ± 0.04
ERA5							
INV height (hPa)	868.7 ± 77.1	864.2 ± 71.0	782.3 ± 97.9	763.3 ± 84.6	837.6 ± 104.1	795.2 ± 94.9	780.6 ± 95.2
INV strength (K.hPa^{-1})	0.16 ± 0.07	0.17 ± 0.07	0.12 ± 0.04	0.13 ± 0.04	0.12 ± 0.04	0.11 ± 0.02	0.11 ± 0.02
II. Cloud statistics							
COARSE							
Total cloud thickness (hPa)	70.6 ± 67.7	28.0 ± 28.9	**103.0 ± 84.3**	52.6 ± 48.4	171.0 ± 103.7	**126.0 ± 95.2**	57.8 ± 62.5

Accepted Article

Cloud top height (hPa)	821.7 ± 112.6	889.4 ± 77.9	**778.7 ± 99.7**	822.1 ± 71.3	728.4 ± 108.3	**757.8 ± 708.1**	758.1 ± 110.2
Cloud base height (hPa)	927.6 ± 49.8	917.3 ± 58.4	922.3 ± 48.4	**890.1 ± 51.0**	**939.3 ± 36.1**	**922.7 ± 51.2**	817.9 ± 81.8
ERA5							
Total cloud thickness (hPa)	65.8 ± 64.4	**21.8 ± 16.2**	98.4 ± 85.1	**44.2 ± 46.7**	**151.5 ± 100.8**	**87.3 ± 81.3**	34.8 ± 36.9
Cloud top height (hPa)	841.5 ± 113.6	**906.2 ± 57.0**	**810.0 ± 102.3**	**862.8 ± 69.2**	**761.0 ± 110.4**	**820.1 ± 88.9**	**807.1 ± 98.1**
Cloud base height (hPa)	934.3 ± 39.2	920.9 ± 48.6	**930.4 ± 39.8**	914.7 ± 42.9	934.4 ± 39.1	918.4 ± 49.9	831.3 ± 84.2

3.2. Inversion

Previous studies over the SO have often revealed that there are large biases in the main inversion, especially on the cold-air side of cyclones (Williams et al., 2013, Lang et al., 2018). Based on T20's cluster framework, we extend our analysis to consider the nature of inversions from 950 to 600 hPa. As discussed in Section 2.2.2, while degrading the vertical resolution from the FINE to COARSE, averaging among layers tends to smooth out the strength of inversions, therefore, an interpolation method was applied instead. Hence, a direct comparison of the main inversion (e.g., its height and strength) between T20 and this work should still be taken cautiously. Table 2 also presents a comparison of the "no inversion" category between the COARSE observation and ERA5. Across all seven clusters, ERA5 displays a greater percentage of soundings having no inversion with a larger bias associated with the colder SSTs (clusters C1 and C2). The weakest bias is in the high-pressure cluster, M1 (4.4%), followed by the warm cluster W1 (6.2%). The inversion strength in the COARSE observation is consistently greater than ERA5 for all clusters, further suggesting that the interpolation algorithm in the reanalysis is potentially smoothing out the inversion. Fig. 3 shows the comparison of the main inversion height between the COARSE observations and ERA5, which are largely consistent. Specifically, the range of correlation coefficients for the warm, moderate, and cold clusters are 0.69, 0.72-0.81 and 0.51-0.74, respectively.

Looking first at the warm cluster, W1, the results indicate that there is a relatively strong correlation between the two products, with a correlation coefficient of 0.69. The main inversion in the COARSE and ERA5 profiles are fairly comparable and at a relatively low altitude of 860.0 hPa and 868.7 hPa with the strength of 0.18 K hPa^{-1} and 0.16 K hPa^{-1}, respectively.

Accepted Article

Accepted Article

Moving to the high-pressure cluster, M1, a strong correlation in the main inversion height is again found between the COARSE and ERA5 profiles. The main inversions are largely located from 950–850 hPa, with a correlation coefficient of 0.72, as expected in a region of strong subsidence like M1. The average inversion heights for the COARSE and ERA5 profiles are 863.0 hPa and 864.2 hPa, with the corresponding average strengths of 0.18 K hPa^{-1} and 0.17 K hPa^{-1}, respectively.

Considering clusters M2, M3, and M4, the first noticeable feature is that the average altitude of the main inversion spreads broadly from 950 to 600 hPa (Fig. 3), and the strength of the inversion is smaller compared to clusters W1 and M1 (Table 2), possibly owing to low-level convergence/instability generated by cyclone dynamics. Interestingly, ERA5 reflects these characteristics well. Perhaps the single most striking point is that the main inversion derived from ERA5 profile in the post-frontal cluster (M3) agrees reasonably well to the COARSE profile, with a correlation coefficient of 0.75. We note that previous studies evaluating the height of the MABL found that the ERA-Interim reanalysis underestimated the height against atmospheric soundings in the post-frontal environment over Macquarie Island (Lang et al., 2018, Hande et al., 2014). It is encouraging to see such an improvement in ERA5 dataset.

The inversion for cluster C1 is similar to that of M4. Both of these clusters are associated with low MSLP suggesting low-level convergence/instability. While there appears to be a high correlation between the COARSE and ERA5 profiles, a comparison to the FINE profiles (T20) indicated that the main inversion height is underestimated in both the COARSE and ERA5 profiles. Finally, turning to the Antarctic coastline cluster, C2, it shows the lowest correlation coefficient (r=0.51). This weak correlation suggests that the thermodynamic structure of the Antarctic coastline air mass is not well represented in ERA5, which could potentially be due to the misrepresentation of the dry, descending katabatic outflows, interacting with large-scale horizontal advection (Dong et al., 2020). Given that our discussions are merely based on the maximum gradient of virtual potential temperature, $d\theta_V/dp$ from 950 to 600 hPa, the results from the inversion analysis find that the slopes of the regression lines (e.g., red line) are always less than one-to-one lines (e.g., black line) for all clusters. On average, the inversion heights are being moderated in ERA5.

Accepted Article

3.3. Cloud layers

One of our primary interests is to investigate whether ERA5 represents the cloud macrophysics across the SO as reported in T20, specifically the number of inferred cloud layers (no cloud, one layer, two layers, three layers and solid cloud) between 950 and 600 hPa. To achieve this, we construct contingency tables of the number of inferred cloud layers for each cluster. Values along the upper-right diagonal denote agreement in the cloud structure between the two representations. Values in the upper-left and lower right portions of the tables denote structural differences in the number of inferred cloud layers between the two representations. Given the potential importance of thin cloud layers to the radiative transfer, we explicitly consider the effect of vertical resolution (FINE vs. COARSE observations) before exploring the effect of reanalysis algorithm (COARSE observations vs ERA5).

To explore the sensitivity of our analysis to the vertical resolution of both the observations and ERA5 product, we repeated the analysis across a range of resolutions, namely FINE and COARSE resolution for the observations and at 137 and 37 pressure levels for ERA5. Different pathways for the interpolation were considered (e.g., observations were linearly interpolated to 37 levels directly from the raw observations, the FINE resolution and from 137 ERA5 pressure levels.) We also explored the difference between using linear interpolation and averaging when degrading the resolution from 137 vertical levels to 37. Our results were not sensitive to the resolution when linear interpolation was used. We found, however, that averaging from 137 ERA5 pressure levels to the corresponding 37 ERA5 pressure levels smoothed the profiles, which affected the results.

Looking first at cluster M1, a single layer of cloud was most commonly recorded, which is consistent with strong subsidence over the lower latitudes of the SO (see T20 for a full synoptic analysis). Both the FINE and COARSE resolution profiles (Fig. 4b) predominantly capture this single layer structure, with 56.2% of all profiles recording one single cloud layer at either resolution. Overall, 82.7% of the profiles fall along the diagonal, indicating that structure was not sensitive to the resolution. Not surprisingly, when changes do occur (e.g., not in the diagonal line), they predominantly reduce the number of cloud layers at COARSE resolution (13.5%). A small percentage of soundings show more cloud layers (3.7%) at COARSE resolution.

Accepted Article

For the remaining six clusters, the same basic principle holds: the number of cloud layers is not particularly sensitive to the resolution, but when changes do occur, fewer cloud layers are evident at COARSE resolution. Clusters M2 (frontal), M4 (warm front) and C1 (high-latitude SO) show the greatest sensitivity to resolution with the greatest reduction in the number of cloud layers at COARSE resolution (27.9, 31.5 and 28.5% for M2, M4, and C1, respectively). This is not particularly surprising, either, as these clusters commonly have more clouds above the main inversion in the lower free troposphere (Fig. 2), consistent with the synoptic meteorology established in T20.

Turning to the comparison between the COARSE profiles and ERA5 profiles (Fig. 4h-n), we again observe a systematic bias with a reduction in the number of cloud layers in ERA5 profiles for six of the seven clusters with the exception being cluster C2 (Antarctic coast). Looking first at cluster W1, we see that 68.8% of all W1 soundings have the same structure in either profile, 22.6% of the soundings have more cloud layers in the COARSE resolution representation and the remaining 8.6% of the soundings have more clouds layers in ERA5 representation. Given that the COARSE and ERA5 profiles are at the same resolution (37 levels), the biases cannot only be attributed to resolution, rather the differences very likely arise in the construction of ERA5. Looking further into the higher latitude clusters (M2-C1), a similar bias was also identified despite there being a good agreement in the frequency of the number of cloud layers [M2 (52.6%), M3 (58.7%), M4 (58.4%), and C1 (52.5 %)]. For example, there was also a large percentage of the M2 (37.5%), M3 (30.4%), M4 (31.2%) and C1 (39.9%) soundings having more cloud layers in COARSE than ERA5, respectively. These large discrepancies, particularly for clusters in the vicinity of the cyclone center (M2-C1), contributed to greater bias in cloud geometric thickness (e.g., thinner) and cloud top height (lower) in ERA5 (Table 2) compared to that of both the FINE and COARSE observations (T20). For instance, the cloud top height and cloud thickness in ERA5 is remarkably shallower (820.1 hPa) and thinner (87.3 hPa) in cluster C1 than that of COARSE resolution which are 752.2 and 124.9 hPa, respectively. The remaining 9.9, 10.9, 10.5 and 7.6 % of the M2, M3, M4 and C1 soundings have more cloud layers in ERA5 than in COARSE. The cloud macrophysics change dramatically when moving from C1 to C2. Along the Antarctic coast, cloud-free conditions (61.2%) dominate with ERA5 profiles having more cloud layers 20.9% of the time and fewer cloud layers 2.2% of the time. For cloud-free conditions, a small percentage of no-cloud is observed in the moist clusters M4 (2.7%), C1

(4.1%), W1 (10%) and M2 (11.6%) between the two representations. Not surprisingly, the high-pressure (M1) and post-frontal (M3) clusters account for the second and third largest no-cloud regimes. To test the significance of ~28.3% more cloud layer in COARSE to ERA5 (i.e. total percentage of all clusters in upper left triangle in Fig. 4h-n) , we ran different Monte Carlo simulations with 50, 100, 150, and 200 binary numbers randomly selected with replacement from the total 2186. We denoted 1 if COARSE has more cloud layer than ERA and 0 otherwise. The simulations are repeated with different number of times of 500, 1000, 10000, and 100000. All results found indicate that 28.3% more cloud layer is statistically significant with 95% confidence.

In summary, when using the dewpoint depression as a proxy for a cloud layer, we found that ERA5 tends to have less cloud thickness than the observations, which can be traced back to the differences in vertical resolution and the reanalysis algorithm itself. The former cause is in line with the work of Atlas et al., 2021 in which we may need higher vertical resolution (e.g., 50 m below 500 hPa) to resolve a 200 m cloud layer thickness commonly found over the SO. The latter cause is strengthened by the systematic bias in ERA5 dewpoint temperatures (i.e., bias of ERA5 specific humidity) as discussed in Section 3.1.

4. Radiative sensitivity to cloud macrophysics

In this section, two representative case studies are presented to investigate the sensitivity of radiative transfer to cloud macrophysics (e.g., cloud layer, cloud top height) to better understand the impacts of vertical resolution on the radiation at the surface (SFC) and the top of the atmosphere (TOA). The representative cases were selected based on the following sequential-order criteria: in the daytime, close to cluster centroid and multi-layer cloud structure (for C1). To accomplish this, we run the radiative transfer model on observed and reanalysis profiles in the high-latitude Southern Ocean (C1) and the postfrontal environment (M3) clusters.

4.1 High-Latitude Southern Ocean (C1)

The observed profile, measured at 21:56 UTC 15 February 2018, was taken from the CAPRICORN 2018 campaign when the RV Investigator was at 132.0°E and 58.5°S. The profile

Accepted Article

provides the pressure, temperature, water vapor, ozone concentration (acquired from ERA5) as model inputs to calculate the SW and LW flux vertical profiles.

Table 3. The calculated shortwave/longwave radiative fluxes

	Pressure level (hPa)	Shortwave downward flux (Wm^{-2})	Shortwave direct flux (Wm^{-2})	Shortwave diffuse flux (Wm^{-2})	Longwave downward flux (Wm^{-2})	Longwave upward flux (Wm^{-2})
Example 1 – Hight latitude Southern Ocean (C1) – 21:56 UTC 15 February 2018						
FINE	TOA	358.4	358.4	0	0	205.9
	SFC	46.1	0	46.1	311.2	324.1
COARSE	TOA	358.4	358.4	0	0	212.6
	SFC	90.5	0.3	90.2	302.5	323.9
ERA5	TOA	358.4	358.4	0	0	212.4
	SFC	95.9	0.4	95.5	305.8	324.0
Example 2 – Postfrontal Environment (M3) – 04:00 UTC 18 February 2018						
FINE	TOA	931.9	931.9	0	0	245.2
	SFC	353.6	0.1	353.5	314.4	333.5
COARSE	TOA	931.9	931.9	0	0	247.5
	SFC	462.4	0.3	462.1	312.3	333.5
ERA5	TOA	931.9	931.9	0	0	247.6
	SFC	462.2	0.3	461.9	312.3	332.5

Fig. 5a shows vertical profiles at different resolutions of FINE, COARSE and ERA5. It can be seen from the observed profile (blue) that the multi-layered cloud appears to be at four different layers of the lower troposphere including 890–860, 770–755, 690–670 and 655–560 hPa. While moving from FINE to COARSE resolution, the COARSE profile fails to capture the inferred cloud layer at 690–670 hPa seen in the FINE profile. Therefore, three layers of cloud are detected in the COARSE profile. On the contrary, ERA5 profile only captures two layers of cloud in the low-level troposphere. Motivated by these profiles, we set up three different scenarios as FINE, COARSE, and ERA5, respectively (Sub-Table 2) for the radiative transfer simulations. At the COARSE resolution, a layer of cloud is assumed to be 10 hPa thick if only one vertical grid point meets the cloud layer criteria.

Fig. 6 shows the calculated SW, LW fluxes and their associated heating/cooling rate profiles. The cloud layer thicknesses are indicated as light red/blue (ice/water layer) shaded areas (Fig. 6a-c, 6f-h). For a water cloud layer, the optical depth is estimated using equation (1). As the cloud top height and temperature (CTT) of the top-most cloud layer in FINE was at 4268.6 m and -17.6 °C, we assumed this top cloud layer is an ice cloud and its optical depth is 10. The CTT is consistent with the collocated CTT from Himawari-8 satellite product (Huang et al.,

Accepted Article

2019, not shown). The optical depth is selected based on the total cloud visible optical depth in the CERES data at the ship location (i.e., 22.13). Therefore, the total cloud optical depth in FINE due to 4 layers of cloud is 22.09 (Sub-Table 2). For COARSE and ERA5, the ice cloud optical depth is assumed to be linearly decreased from a value of 10 as a function of layer geometric thickness. To facilitate the comparison of the three experiments, the cloud microphysics taken from CERES data (e.g., ice/water particle radius) are kept the same. We note that these values are comparable to satellite and field observations previously reported over the SO (Huang et al., 2016; Chubb et al., 2016).

The amount of incoming radiation at TOA is 358.4 Wm^{-2} for the three experiments. Not surprisingly, the FINE results in the least amount of the downward SW surface flux (i.e., 981.1 hPa), which is 46.1 Wm^{-2}. The large attenuation of the SW flux (181.9 Wm^{-2}) is primarily attributed to the relatively thick ice cloud layer at 655 – 560 hPa in this case (Fig. 6d). The SW downward flux further decreases as it goes through the liquid cloud layers. The total transmittance through the atmosphere is the sum of the direct (dash-dotted line) and diffuse (dashed line) transmittances (Fig. 6a-c). For instance, while the direct flux in Fig. 6a decreases exponentially, the diffuse flux increases. The diffuse flux increases to 167.1 Wm^{-2} at 590 hPa, then decreases, indicating that absorption is significant in the ice cloud layer.

Moving to COARSE, the simulated downward SW surface flux is 90.5 Wm^{-2}. ERA5 showed the largest amount of the downward SW flux (95.9 Wm^{-2}) at the surface. The difference of the simulated downward SW surface flux between ERA5 and FINE is 49.8 Wm^{2}. As ERA5 fails to capture two cloud layers at 770 and 690 hPa (Fig. 6a), no significant reduction of the downward SW surface flux was produced at that level. This result accentuates the impact of a thin layer of cloud on the radiative transfer. Overall, the attenuation of SW radiation by clouds has been underestimated due to the course resolution of ERA5. Figure 6e shows the SW heating rate profiles for the three experiments. The maximum heating rate from the surface up to 200 hPa for FINE, COARSE, and ERA5 are 4.3, 2.5, and 2.5 K day^{-1}, respectively.

Considering the surface LW radiation fluxes, FINE has the largest amount of downward LW flux (311.2 Wm^{2}) at the surface and the least amount of outgoing LW flux (205.9 Wm^{2}) at the TOA. As the upward LW radiation reaches the cloud tops (e.g., colder temperature), its intensity decreases (Fig. 6f-h). Figure 6j shows the LW heating rate profiles for the three

Accepted Article

experiments. Since there is a net cooling (e.g., negative values), it is suggested that emission dominates absorption. The cooling-to-space effect is significant at cloud-top altitudes, with maximum cooling rates from surface up to 200 hPa for FINE, COARSE, and ERA5 of -27.7, -14.9 and -13.5 K day^{-1}. Unsurprisingly, for water cloud layers with large optical depth (e.g., large LWP), LW radiative heating is seen near cloud bases with the heating rates approaching 5.1 and 3.7 K day^{-1} (760 and 865 hPa, respectively) for FINE case and 3.8 K day^{-1} (745 hPa) COARSE, respectively.

4.2 Postfrontal Environment (M3)

It is of particular interest to investigate how the macrophysics impacts the surface radiation in the postfrontal environment over the SO. To assess this, the observed profile (launched at 141.5°E and 56.6°S), also taken from the CAPRICORN 2018 campaign at 04:00 UTC 18 February 2018, was examined. Fig 5b. shows vertical profiles at different resolutions of FINE, COARSE and ERA5. It can be seen from the observed profile (blue) that a layer of cloud appears to be at 900 – 865 hPa. While both COARSE and ERA5 well represent the observed cloud layer, their cloud thicknesses are smaller (900 – 875 hPa). Hence, the main inversion in the FINE observation (860 hPa) is higher compared to that of COARSE and ERA5 (880 hPa). Analogous to section 4.1, we set up three different scenarios as the FINE, COARSE, and ERA5 (Sub-Table 2).

Fig. 7 shows the calculated SW, LW fluxes and its associated heating/cooling rate profiles. The cloud layer thicknesses are indicated as light blue (water cloud layer) shaded areas (7a-c, 7f-h). The amount of incoming radiation at TOA is 931.9 Wm^{-2} for the three experiments. As expected, the least amount of the downward SW surface flux at the surface (353.6 Wm^{2}) occurs for FINE. The amount of the downward SW surface flux for COARSE and ERA5 is 462.5 Wm^{2} and 462.2 Wm^{2}, respectively. The small difference between COARSE and ERA5 results can be due to the variation of the water vapor mixing ratio and temperature between the two profiles. The difference of the downward SW surface flux between ERA5 and FINE is 108.6 Wm^{2}. Figure 7e shows the SW heating rate profiles for the three experiments. The maximum heating rates from the surface up to 200 hPa for FINE, COARSE, and ERA5 are 16.7, 18.6, and 18.7 K day^{-1}, respectively. The results suggest that strong SW heating due to solar absorption is common in the cloud layers.

Accepted Article

Moving to the LW radiation, FINE has the largest amount of the downward LW surface flux (314.4 Wm^2) and the least amount of the outgoing LW radiation (245.2 Wm^2) at the TOA. Figure 7j shows the LW heating rate profiles for the three experiments. The cooling-to-space effect is significant at cloud-top altitudes, with maximum cooling rates for FINE, COARSE, and ERA5 of -38.6, -61.1 and -62.6 K day^{-1}, respectively. As with the C1 example, LW radiative heating is seen near the cloud base in FINE with the heating rate nearly 9.6 K day^{-1} (885 hPa). This is because the LWP in FINE is larger than it is in COARSE and ERA5 case (Sub-Table 2). Our RTM's result is consistent with Turner et al., (2018) in which greater LW radiative heating near cloud base was found when a liquid cloud layer having larger LWP (e.g., larger than 30 g m^{-2}).

Finally, potential shortcomings of the analysis need to be considered. First, although it is possible to speculate that a cloud is optically thick ($\tau > 1$) and multiple scattering dominates single scattering since diffuse transmittance is a major contributor to the total transmittance once the solar radiation reaches cloud-top (Fig. 7a). Quantitatively distinguishing the contribution of the single and multiple scattering remains a challenge due to the uncertainty in cloud properties. Second, no aerosol is considered, therefore, the potential for either enhanced or attenuated radiation due to absorption or scattering of aerosols is not represented. Third, it is well-documented that the cloud microphysics (e.g., the lack of supercooled liquid water in mixed-phased clouds in climate models) plays an important role in driving the radiation bias over the SO (Bodas-Salcedo et al., 2014, 2016). For simplicity, we have only categorized the inferred cloud layers into either ice or liquid phase. Such settings, as well as the resulting fluxes and heating profiles, may not perfectly match the real-world scenarios. Notwithstanding, we compared the RTM outputs (e.g., downward SW surface flux) against the CERES data and found that our RTM results are reasonable (Sub-Table 3). As a focus of this study is on the representation of thin cloud layers over the SO and sensitivity of radiative transfer to such clouds, we consider these examples to only be illustrative and not definitive. A deeper appreciation of the potential bias in radiative forcing over the SO would need to consider both cloud macrophysics and microphysics. We are strictly interested in the impact of cloud macrophysics here and have demonstrated that a finer vertical resolution can help to better represent the inversion level and cloud layer as well as to reduce the amount of downward shortwave surface radiation in a physically based manner.

Accepted Article

Accepted Article

5. Discussion and conclusion

In this study, we evaluated the low-level thermodynamic structure of the marine atmospheric boundary layer (MABL) including inferred cloud layers and inversions in ERA5 vertical profiles against the 2186 observed high-resolution soundings. We were particularly keen to explore the cloud macrophysics over the high latitudes of the Southern Ocean, where the greatest bias in surface radiation is located. Accordingly, the data were further sorted based on the synoptic clustering established in T20. To illustrate the potential impacts of any bias in ERA5 thermodynamic structure on the radiative budget, we extend our work to investigate the sensitivity of radiative transfer to cloud macrophysics (e.g., cloud layer, cloud top height) by running the NASA Langley Fu-Liou radiative transfer model on two different representative soundings/examples.

Overall, the general characteristics of the mean ERA5 thermodynamic profiles through the 7 clusters are very comparable to that observed, indicating that ERA5 has skill in depicting low-level thermodynamic structures over the SO (T20, Lang et al., 2018), regardless of the synoptic meteorology. This was anticipated as these soundings were employed in the generation of the reanalysis. Our results also suggest that there is still a relatively weak dry/wet bias of dewpoint temperatures (e.g., 0.5-1°C) which is inherited from the bias of specific humidity (Hersbach et al., 2020) in ERA5 lower/upper atmosphere, particularly in the post-frontal cluster M3. This finding is important, because, as the atmosphere is drier (e.g., dewpoint temperature in Fig. 2, cluster M3 from 925-825 hPa), it is less likely that a cloud layer is formed, which in turn results in a larger amount of surface shortwave radiation. Seethala et al., (2021), using relative humidity as a proxy for a cloud layer, also documented that 137 ERA5 pressure levels fail to capture the cloud layer, especially in the late summer. Furthermore, our results concur well with the bias of specific and relative humidity in ERA5 reported in Graham et al. (2019), Vignon et al. (2019) and Seethala et al., (2021) over the Arctic, Antarctic, northwest Atlantic, respectively.

Given the potential importance of multi-layer clouds to the radiative transfer, we further investigate the effect of vertical resolution (FINE vs. COARSE observations) and the effect of reanalysis algorithm (COARSE observations vs ERA5) by conducting a simple cloud layer count between 950 hPa and 600 hPa. For the former, our results show that the number of inferred cloud layers is not particularly sensitive to the resolution, however, fewer cloud layers are evident at COARSE resolution when differences between the two representations were taken into

consideration. For the latter, we found a systematic bias with significant reduction in the number of inferred cloud layers in ERA5 through all clusters except for the Antarctic coast cluster (C2). Given that ERA5 and COARSE profiles are at the same resolution (37 levels), the biases cannot be attributed to resolution, rather the differences very likely arise in the construction of ERA5. Overall, the best agreements in the number of cloud layers between COARSE and ERA5 are found in the high-pressure (M1, 76.8%), Antarctic coast (C2, 77%) and warm clusters (W1, 68.8%) of which 52.2%, 47.8%, and 61.2 % of the profiles record one, one and no cloud layer, respectively according to the observations (Fig4h-i and 4n). For other clusters, a large population of the M2 (37.5%), M3 (30.7%), M4 (31.2%) and C1 (39.9%) soundings have fewer cloud layers in ERA5 than in the COARSE profiles. These differences also contribute to the greater biases in cloud geometric thickness (e.g., thinner) and cloud top height (lower) in ERA5 (Table 2) compared to that of both the COARSE and FINE observations (T20). It is particularly worth noting that the largest differences of cloud geometric thickness and cloud top height in ERA5 are found to reside in the high-latitude Southern Ocean cluster C1 where the simulated radiation bias in climate models (e.g., CMIP3, UM) is the greatest (Trenberth and Fasullo, 2010; Schuddeboom et al., 2019).

A similar analysis on the characteristics of the main inversion has also been carried out. We found that ERA5 displays a greater percentage of soundings having no inversion with a larger bias that tends to be associated with the colder SSTs. Overall, the statistics of the main inversion suggest a good consistency between COARSE and ERA5 with the range of correlation coefficients for the warm, moderate, and cold clusters of 0.69, 0.72-0.81 and 0.51-0.74, respectively. Similar consistency between ERA5 and dropsondes above the Gulf Stream was also reported in Seethala et al., (2021) where ERA5-derived inversion is shallower with the correlation of 0.83 and 0.62 for boreal winter and summer, respectively. We note that the soundings from this campaign were not assimilated into ERA5, in contrast to the 2186 soundings used in this analysis. Our analysis also reveals that the inversion strength in ERA5 is consistently weaker than the COARSE observation for all clusters suggesting that the reanalysis simulation itself is potentially smoothing out and moderating the vertical structure.

Our examination of the sensitivity of radiative transfer to cloud macrophysics suggests that the difference in the amount of downward shortwave surface radiation partially arises from the lack of cloud layers in ERA5 as detailed in Section 3.2. For example, the difference of the

Accepted Article

downward shortwave surface flux can be 49.8 Wm^2 in cluster C1 or as large as 108.6 Wm^2 in cluster M3. As such, we believe that correct representation of thin multiple cloud layers by having a finer vertical resolution (e.g., 50 m below 500 hPa to resolve a 200 m cloud layer) can help to reduce the amount of downward shortwave surface radiation over the SO as reported in Wang et al (2021).

Our analysis uses the dewpoint temperature depression as a proxy for cloud layers to facilitate a direct comparison between the observations and ERA5. Initially, we compared a handful of cases between the the cloud liquid (and/or ice) water content in ERA5 to the observed radar and lidar products during the CAPRICORN 2018 field campaign (not shown), and commonly found that a cloud layer is completely missing from the reanalysis. The lower cloud fraction in ERA5 is also reported in Wang et al., (2020). We propose that further research should be undertaken to comprehensively evaluate ERA5's cloud products against observations (Berry et al., 2019), specifically at the high latitudes over the Southern Ocean. This study has also further highlighted the potential bias of using ERA5 as initial and boundary conditions for regional numerical simulation as discussed in Atlas et al. (2020).

Acknowledgments

This work is supported by an Australian Research Council discovery grant DP190101362. The authors deeply thank the entire CAPRICORN, MARCUS, MICRE and SOCRATES teams for their tremendous efforts and dedication in collecting the datasets. We thank the CSIRO MNF for its great support and service. All observation are currently available at the Earth Observing Laboratory website (https://data.eol.ucar.edu/master_lists/generated/socrates/). The 137 and 37 ERA5 model levels can be downloaded at https://apps.ecmwf.int/data-catalogues/era5/?class=ea&stream=oper&expver=1 and https://cds.climate.copernicus.eu/cdsapp#!/dataset/reanalysis-era5-single-levels?tab=overview, respectively. The collocated soundings and ERA5 dataset and the radiative transfer results can be found at https://bridges.monash.edu/projects/ERA5_Manuscript/126569. The NASA Langley Fu-Liou radiative transfer model can be downloaded from https://web.archive.org/web/20100527152929/http://snowdog.larc.nasa.gov/rose/fu200503/. We sincerely thank Dr. Artur Gevorgyan at Monash University for insightful comments on the work.

Accepted Article

Accepted Article

6. Reference

Atlas, R. L., Bretherton, C. S., Blossey, P. N., Gettelman, A., Bardeen, C., Lin, P., & Ming, Y. (2020). How well do large-eddy simulations and global climate models represent observed boundary layer structures and low clouds over the summertime Southern Ocean? Journal of Advances in Modeling Earth Systems, 12, e2020MS002205. https://doi.org/10.1029/2020MS002205

Bennartz, R., 2007: Global assessment of marine boundary layer cloud droplet number concentration from satellite. J. Geophys. Res., 112, D02201, https://doi.org/10.1029/2006JD007547.

Berry, E., Mace, G. G., and Gettelman, A. (2019). Using A-Train Observations to Evaluate Cloud Occurrence and Radiative Effects in the Community Atmosphere Model during the Southeast Asia Summer Monsoon. Journal of Climate 32, 14, 4145-4165, available from: < https://doi.org/10.1175/JCLI-D-18-0693.1>

Bodas-Salcedo, A., Williams, K. D., Ringer, M. A., Beau, I., Cole, J. N., Dufresne, J.-L., Koshiro, T., Stevens, B., Wang, Z., and Yokohata, T.(2014): Origins of the solar radiation biases over the Southern Ocean in CFMIP2 models, J. Climate, 27, 41–56, https://doi.org/10.1175/JCLI-D-13-00169.1, 2014

Bodas-Salcedo, A., Hill, P., Furtado, K., Williams, K., Field, P., Manners, J., Hyder, P., and Kato, S. (2016): Large contribution of super- cooled liquid clouds to the solar radiation budget of the Southern Ocean, J. Climate, 29, 4213–4228, https://doi.org/10.1175/jcli-d- 15-0564.1, 2016.

Bolton, D., 1980: The computation of equivalent potential temperature. Mon. Wea. Rev., 108, 1046-1053, doi:10.1175/1520-0493(1980)108%3C1046:TCOEPT%3E2.0.CO;2.

CERES Science Team, Hampton, VA, USA: NASA Atmospheric Science Data Center (ASDC), Accessed <SYN1deg-1Hour> at doi:10.5067/Terra+Aqua/CERES/SYN1deg1Hour_L3.004.

Chubb, T., Huang, Y., Jensen, J., Campos, T., Siems, S., & Manton, M. (2016). Observations of high droplet number concentrations in Southern Ocean boundary layer clouds. Atmospheric Chemistry and Physics, 16(2), 971–987. https://doi.org/10.5194/acp□16□971□2016

Costa-Surós, M., Calbó, J., González, J. A., and Long, C. N.: Comparing the cloud vertical structure derived from several methods based on radiosonde profiles and ground-based remote sensing measurements, Atmos. Meas. Tech., 7, 2757–2773, https://doi.org/10.5194/amt-7-2757-2014, 2014.

Doelling, D. R., M. Sun, L. T. Nguyen, M. L. Nordeen, C. O. Haney, D. F. Keyes, P. E. Mlynczak, 2016: Advances in Geostationary-Derived Longwave Fluxes for the CERES Synoptic (SYN1deg) Product, Journal of Atmospheric and Oceanic Technology, **33**(3), 503-521. doi: 10.1175/JTECH-D-15-0147.1.

Dong, X., Wang, Y., Hou, S., Ding, M., Yin, B., and Zhang, Y. (2020). Robustness of the Recent Global Atmospheric Reanalyses for Antarctic Near-Surface Wind Speed Climatology. Journal of Climate 33, 10, 4027-4043, https://doi.org/10.1175/JCLI-D-19-0648.1

Accepted Article

Fu, Q., and K. N. Liou (1992), On the correlated k-distribution method for radiative-transfer in nonhomogeneous atmospheres, J. Atmos. Sci., 49, 2139–2156, https://doi:10.1175/1520-0469(1992)049<2139:OTCDMF>2.0.CO;2.

Fu, Q., and K. N. Liou (1993), Parameterization of the radiative properties of cirrus clouds, J. Atmos. Sci., 50, 2008–2025, https://doi:10.1175/1520-0469 (1993)050<2008:POTRPO>2.0.CO;2.

Fu, Q., K. N. Liou, M. C. Cribb, T. P. Charlock, and A. Grossman (1997), Multiple scattering parameterization in thermal infrared radiative transfer, J. Atmos. Sci., 54, 2799–2812, https://doi:10.1175/1520-0469(1997)054<2799:MSPITI>2.0.CO;2.

Graham, R. M., S. R. Hudson, and M. Maturilli, 2019: Improved performance of ERA5 in Arctic gateway relative to four global atmospheric reanalyses. Geophys. Res. Lett., 46, 6138–6147, https://doi.org/10.1029/2019GL082781.

Guo, J., Zhang, J., Yang, K., Liao, H., Zhang, S., Huang, K., Lv, Y., Shao, J., Yu, T., Tong, B., Li, J., Su, T., Yim, S. H. L., Stoffelen, A., Zhai, P., and Xu, X.: Investigation of near-global daytime boundary layer height using high-resolution radiosondes: First results and comparison with ERA-5, MERRA-2, JRA-55, and NCEP-2 reanalyses, Atmos. Chem. Phys. Discuss. [preprint], https://doi.org/10.5194/acp-2021-257, in review, 2021.

Hande, L. B., Siems, S. T., Manton, M. J., & Belusic, D. (2012). Observations of wind shear over the Southern Ocean. Journal of Geophysical Research, 117, D12206. https://doi.org/10.1029/2012JD017488

Hersbach H, Bell B, Berrisford P, et al. The ERA5 global reanalysis. Q.J.R. Meteorol. Soc.. 2020;1–51. https://doi.org/10.1002/qj.3803

Huang, Y., Siems, S., Manton, M., Protat, A., Majewski, L., and Nguyen, H. (2019). Evaluating Himawari-8 Cloud Products Using Shipborne and CALIPSO Observations: Cloud-Top Height and Cloud-Top Temperature. Journal of Atmospheric and Oceanic Technology 36, 12, 2327-2347, available from: < https://doi.org/10.1175/JTECH-D-18-0231.1>

Huang Y., S. T. Siems, M. J. Manton, D. Rosenfeld, R. Marchand, G. M. McFarquhar, and A. Protat, 2016: What is the role of sea surface temperature in modulating cloud and precipitation properties over the Southern Ocean? J. Climate, 29, 7453– 7476, https://doi.org/10.1175/JCLI-D-15-0768.1.

Huang, Y., Siems, S. T., Manton, M. J., Hande, L. B., & Haynes, J. M. (2012). The structure of low-altitude clouds over the Southern Ocean as seen by CloudSat. Journal of Climate, 25(7), 2535–2546. https://doi.org/10.1175/JCLI-D-11-00131.1

Klekociuk, A. R., French, W. J. R., Alexander, S. P., Kuma, P., and McDonald, A. J.: The state of the atmosphere in the 2016 southern Kerguelen Axis campaign region, Deep-Sea Res. Pt. II, Volume 174, April 2020, https://doi.org/10.1016/j.dsr2.2019.02.001.

Kuma, P., McDonald, A. J., Morgenstern, O., Alexander, S. P., Cassano, J. J., Garrett, S., Halla, J., Hartery, S.,Harvey, M. J., Parsons, S., Plank, G., Varma, V., and Williams, J.: Evaluation of Southern Ocean cloud in the HadGEM3 general circulation model and MERRA-2 reanalysis using ship-based observations, Atmos. Chem. Phys., 20, 6607–6630, https://doi.org/10.5194/acp-20-6607-2020, 2020.

Accepted Article

Lang, F., Huang, Y., Siems, S. T., & Manton, M. J. (2018). Characteristics of the marine atmospheric boundary layer over the Southern Ocean in response to the synoptic forcing. Journal of Geophysical Research: Atmospheres, 123, 7799–7820. https://doi.org/10.1029/2018JD028700

Li, J., Yi, Y., Minnis, P., 2011. Radiative effect differences between multi-layered and single-layer clouds derived from CERES, CALIPSO, and CloudSat data. J. Quant. Spectrosc. Radiat. Transf. 112, 361–375.

Li, J., Huang, J., Stamnes, K., Wang, T., Lv, Q., Jin, H., 2015. A global survey of cloud overlap based on CALIPSO and CloudSat measurements. Atmos. Chem. Phys. 15, 519–536.

Mace, G. G., Zhang, Q., Vaughan, M., Marchand, R., Stephens, G., Trepte, C., & Winker, D. (2009). A description of hydrometeor layer occurrence statistics derived from the first year of merged Cloudsat and CALIPSO data. Journal of Geophysical Research, 114, D00A26. https://doi.org/10.1029/2007JD009755

Mace, G. G., & Protat, A. (2018a). Clouds over the Southern Ocean as observed from the R/V investigator during CAPRICORN. Part I: Cloud occurrence and phase partitioning. Journal of Applied Meteorology and Climatology, 57(8), 1783–1803. https://doi.org/10.1175/ JAMC-D-17-0194.1

Manton, M. J., Huang, Y., and Siems, S. T. (2020). Variations in Precipitation across the Southern Ocean. Journal of Climate 33, 24, 10653-10670, available from: <https://doi.org/10.1175/JCLI-D-20-0120.1>

McFarquhar, G., Bretherton, C., Marchand, R., Protat, A., Demott, P., Alexander, S., et al. (2020). Observations of clouds, aerosols, precipitation, and surface radiation over the southern ocean: An overview of CAPRICORN, MARCUS, MICRE and SOCRATES. Bulletin of the American Meteorological Studies.

McKay, R.C., Arblaster, J.M., Hope, P. et al. Exploring atmospheric circulation leading to three anomalous Australian spring heat events.Clim Dyn (2021). https://doi.org/10.1007/s00382-020-05580-0

Meyer, K., Yang, P., and Gao, B.-C.: Tropical ice cloud optical depth, ice water path, and frequency fieldsfrom the MODIS level- 3 data, Atmos. Res., 85, 171–182, 2007. https://doi.org/10.1016/j.atmosres.2006.09.009

Minnis, P., S. Sun-Mack, Y. Chen, F.-L. Chang, C.R. Yost, W.L. Smith, Jr., P.W. Heck, R.F. Arduini, S.T. Bedka, Y. Yi, G. Hong, Z. Jin, D. Painemal, R. Palikonda, B. Scarino, D.A. Spangenberg, R.A. Smith, Q.Z. Trepte, P. Yang, and Y. Xie, 2021: CERES MODIS cloud product retrievals for Edition 4, Part I: Algorithm changes. IEEE Trans. Geosci. Remote Sens., 51, no. 4, 2744-2780, doi:10.1109/TGRS.2020.3008866.

Naud, C. M., Booth, J. F., & Del Genio, A. D. (2014). Evaluation of ERA□Interim and MERRA cloudiness in the Southern Ocean. Journal of Climate, 27(5), 2109–2124. https://doi.org/10.1175/JCLI□D□13□00432.1

Sato, K., J. Inoue, S. P. Alexander, G. McFarquhar, and A. Yamazaki, 2018b: Improved reanalysis and prediction of atmospheric fields over the Southern Ocean using campaign-based radiosonde observations. Geophys. Res. Lett., 45, 112406–112413, https://doi.org/10.1029/2018GL079037.

Schuddeboom, A., Varma, V., McDonald, A. J., Morgenstern, O., Harvey, M., Parsons, S., et al. (2019). Cluster□based evaluation of model compensating errors: A case study of cloud radiative effect in the Southern Ocean. Geophysical Research Letters, 46, 3446–3453. https:// doi.org/10.1029/2018GL081686

Seethala, C., Zuidema, P., Edson, J., Brunke, M., Chen, G., Li, X.-Y., et al. (2021). On assessing ERA5 and MERRA2 representations of cold-air outbreaks across the Gulf Stream. Geophysical Research Letters, 48, e2021GL094364. https://doi.org/10.1029/2021GL094364

Trenberth, K. E., & Fasullo, J. T. (2010). Simulation of present□day and twenty□first□century energy budgets of the Southern Oceans. Journal of Climate, 23(2), 440–454. https://doi.org/10.1175/2009JCLI3152.1

Truong, S. C. H., Huang, Y., Lang, F., Messmer, M., Simmonds, I., Siems, S. T., & Manton, M. J. (2020). A climatology of the marine atmospheric boundary layer over the Southern Ocean from four field campaigns during 2016–2018. Journal of Geophysical Research: Atmospheres, 125, e2020JD033214. https://doi.org/ 10.1029/2020JD033214

Turner, D. D., M. D. Shupe, and A. B. Zwink. " Characteristic Atmospheric Radiative Heating Rate Profiles in Arctic Clouds as Observed at Barrow, Alaska". Journal of Applied Meteorology and Climatology 57.4 (2018): 953-968. <https://doi.org/10.1175/JAMC-D-17-0252.1>.

Vignon, É., O. Traullé, and A. Berne, 2019: On the fine vertical structure of the low troposphere over the coastal margins of East Antarctica. Atmos. Chem. Phys., 19, 4659–4683, https:// doi.org/10.5194/acp-19-4659-2019.

Wang, H.; Klekociuk, A.R.; French, W.J.R.; Alexander, S.P.; Warner, T.A. Measurements of Cloud Radiative Effect across the Southern Ocean (43° S–79° S, 63° E–158° W). Atmosphere 2020, 11, 949. https://doi.org/10.3390/atmos11090949

Wielicki, B. A., B. R. Barkstrom, E. F. Harrison, R. B. Lee III, G. L. Smith, and J. E. Cooper, 1996: Clouds and the Earth's Radiant Energy System (CERES): An Earth Observing System Experiment, Bull. Amer. Meteor. Soc., **77**, 853-868. doi: 10.1175/1520-0477(1996)077<0853:CATERE>2.0.CO;2.

Williams, K. D., Bodas□Salcedo, A., Déqué, M., Fermepin, S., Medeiros, B., Watanabe, M., et al. (2013). The transpose□AMIP II experiment and its application to the understanding of Southern Ocean cloud biases in climate models. Journal of Climate, 26(10), 3258–3274. https://doi.org/10.1175/JCLI□D□12□00429.1

Accepted Article

Accepted Article

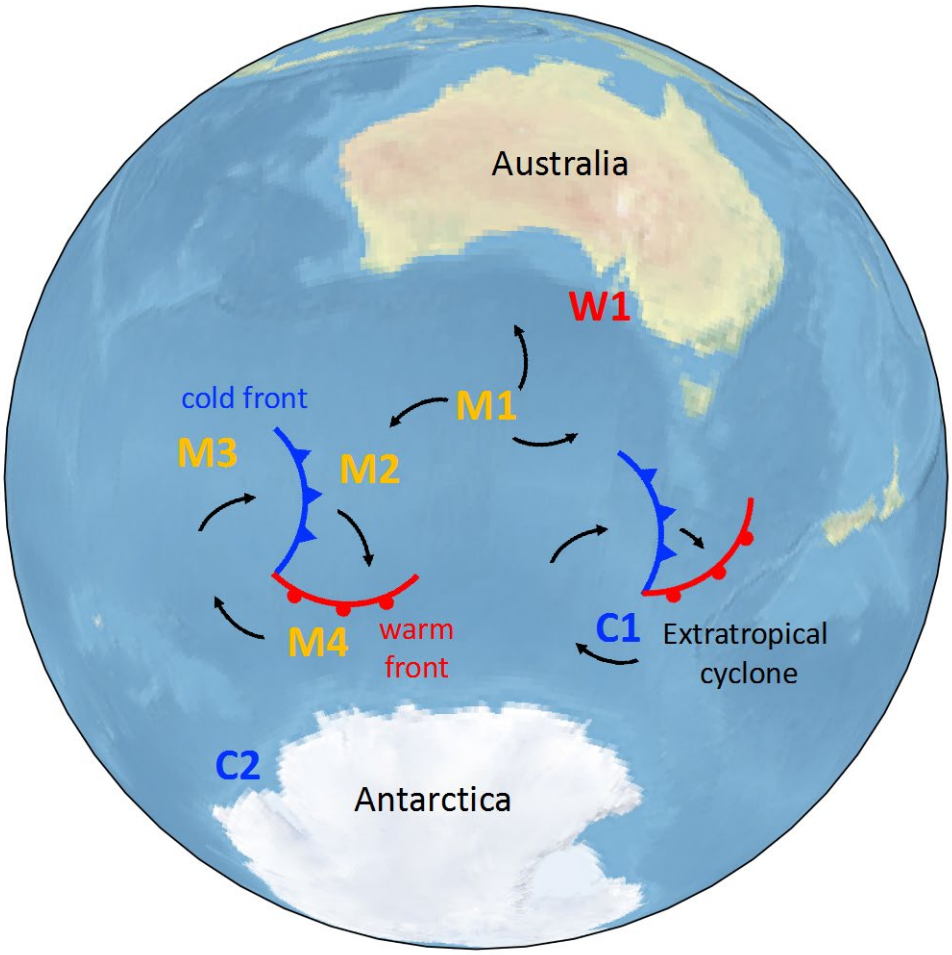

Figure 1. Conceptual illustration of the seven clusters from W1 to C2 over the Southern Ocean derived in T20.

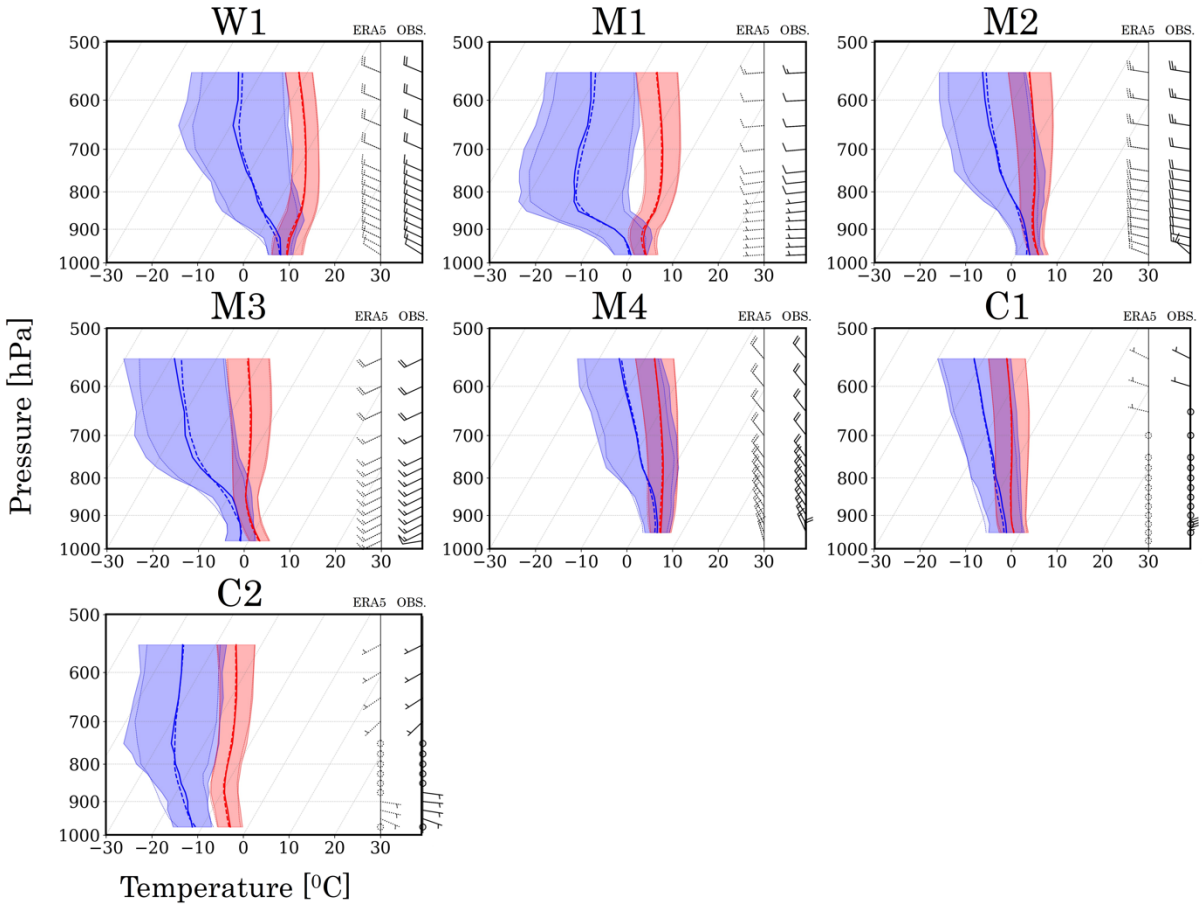

Figure 2. Mean profiles of temperature (red lines), dew point temperature (blue lines), and wind vector for the seven clusters: W1, M1-M4, and C1-C2, displayed as skew-T logP diagrams, shaded region indicating one standard deviation. The solid and dashed lines represent the observations and ERA5, respectively.

Accepted Article

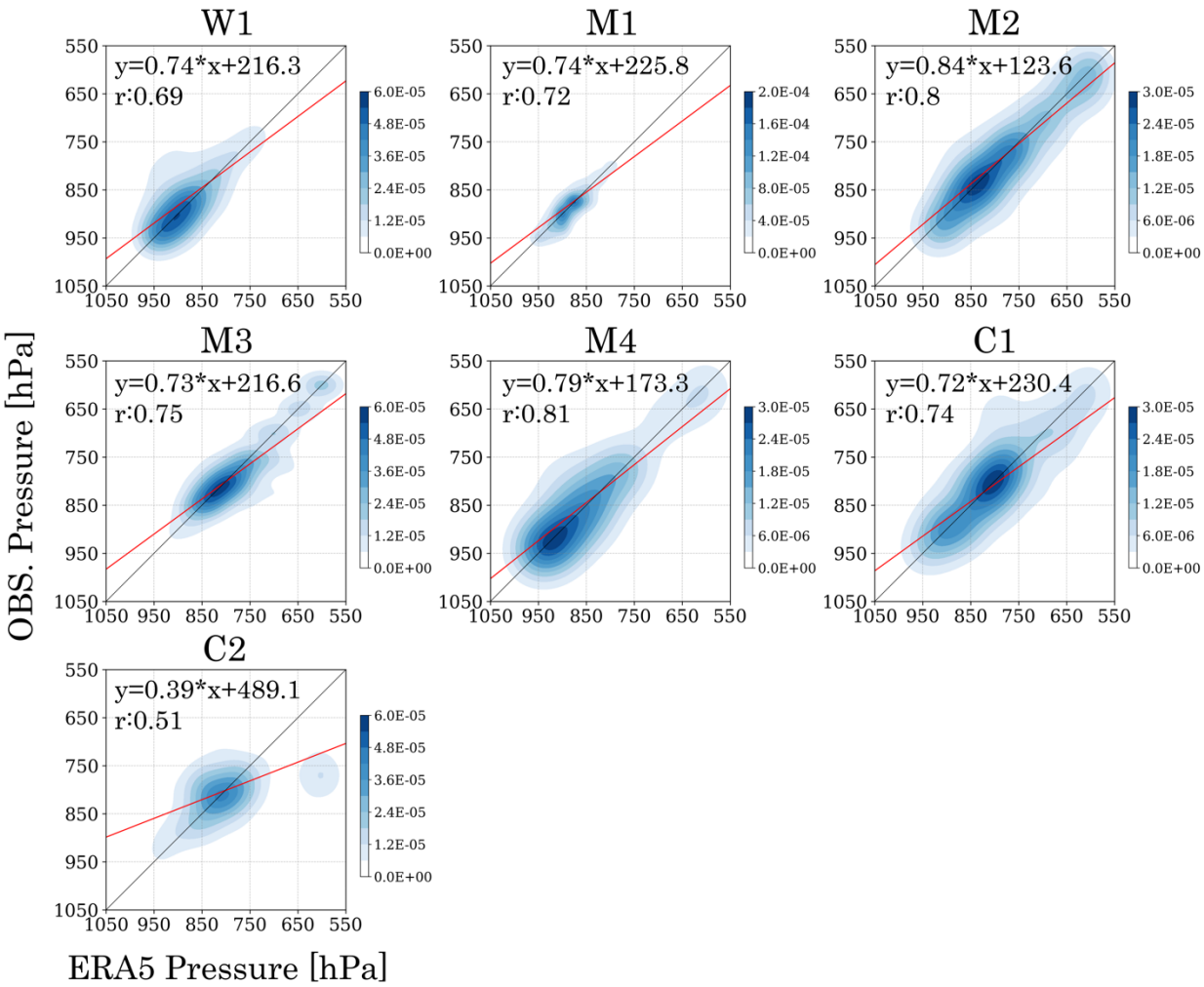

Figure 3. Frequency density plots of the main inversion derived from COARSE observation and ERA5 for the seven clusters: W1, M1–M4, C1, and C2. The black and red lines indicate the one-to-one and regression lines, respectively. Note the "no inversion" category is excluded in these plots.

Accepted Article

Accepted Article

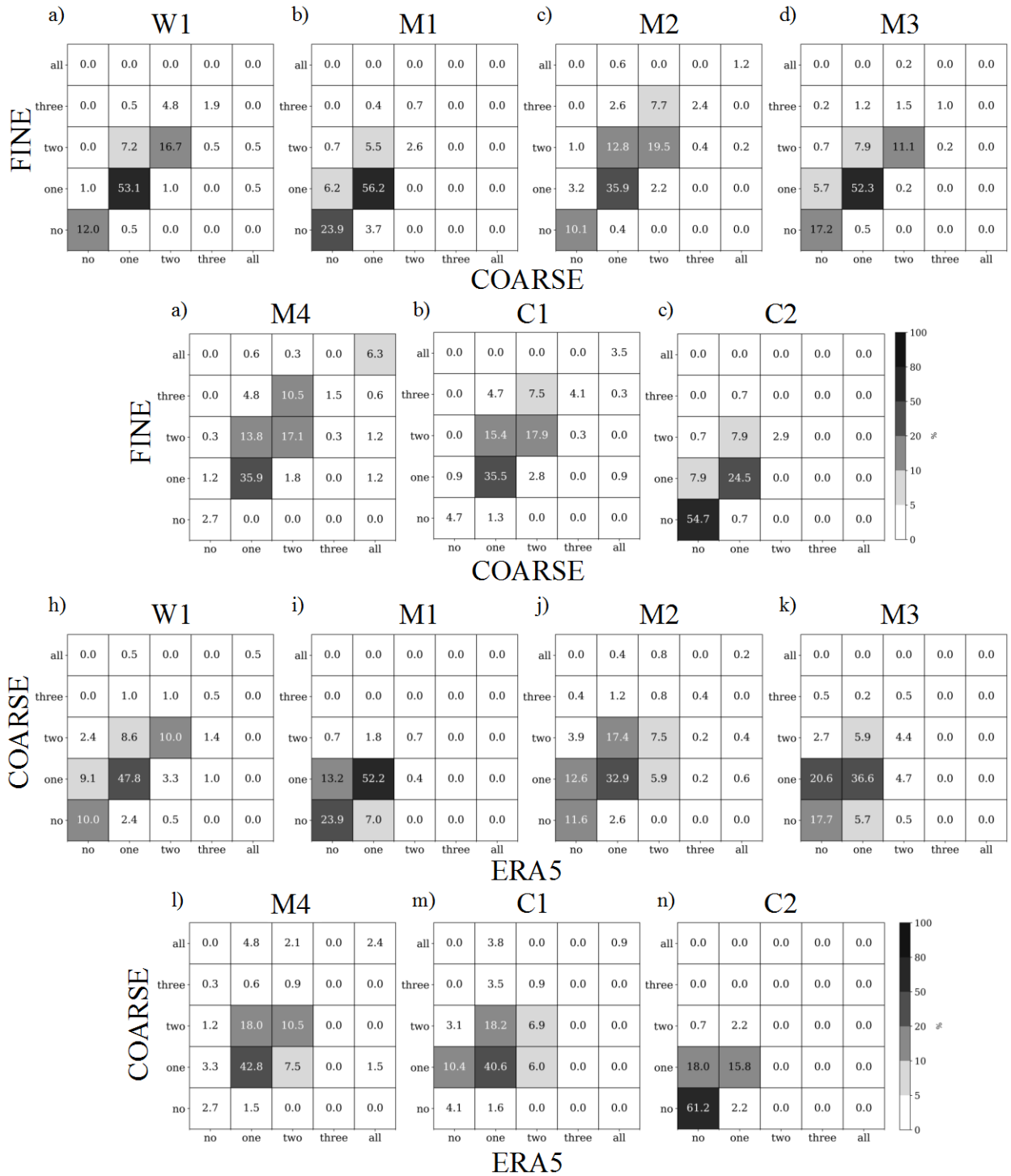

Figure 4. Contingency tables for the number of cloud layers for each of the seven clusters. (a-g) FINE and COARSE resolution observation and (h-n) COARSE observation and ERA5. The numbers indicate percentages and its meaning is the same as underlying shaded colors.

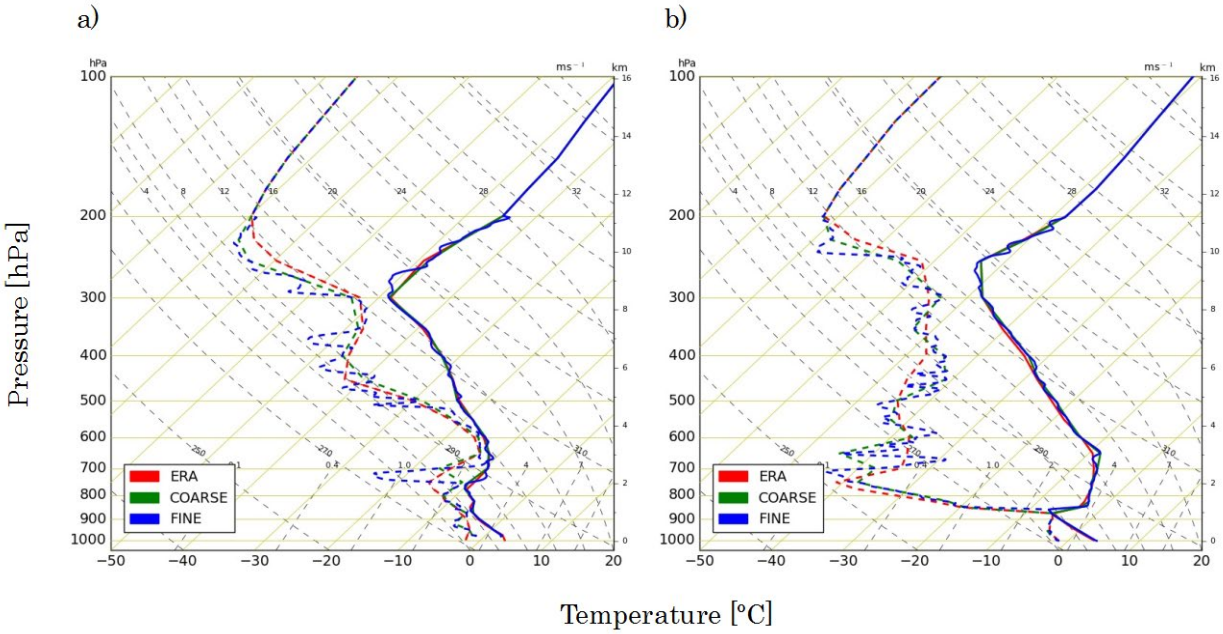

Figure 5. a) The vertical profiles of temperature (solid lines), dew point temperature (dashed lines) for the FINE (blue), COARSE (green), ERA5 (red) displayed as skew-T logP diagrams at 21:56 UTC 15 February 2018. b) As for Figure 5 (a) but at 04:00 UTC 18 February 2018.

Accepted Article

Accepted Article

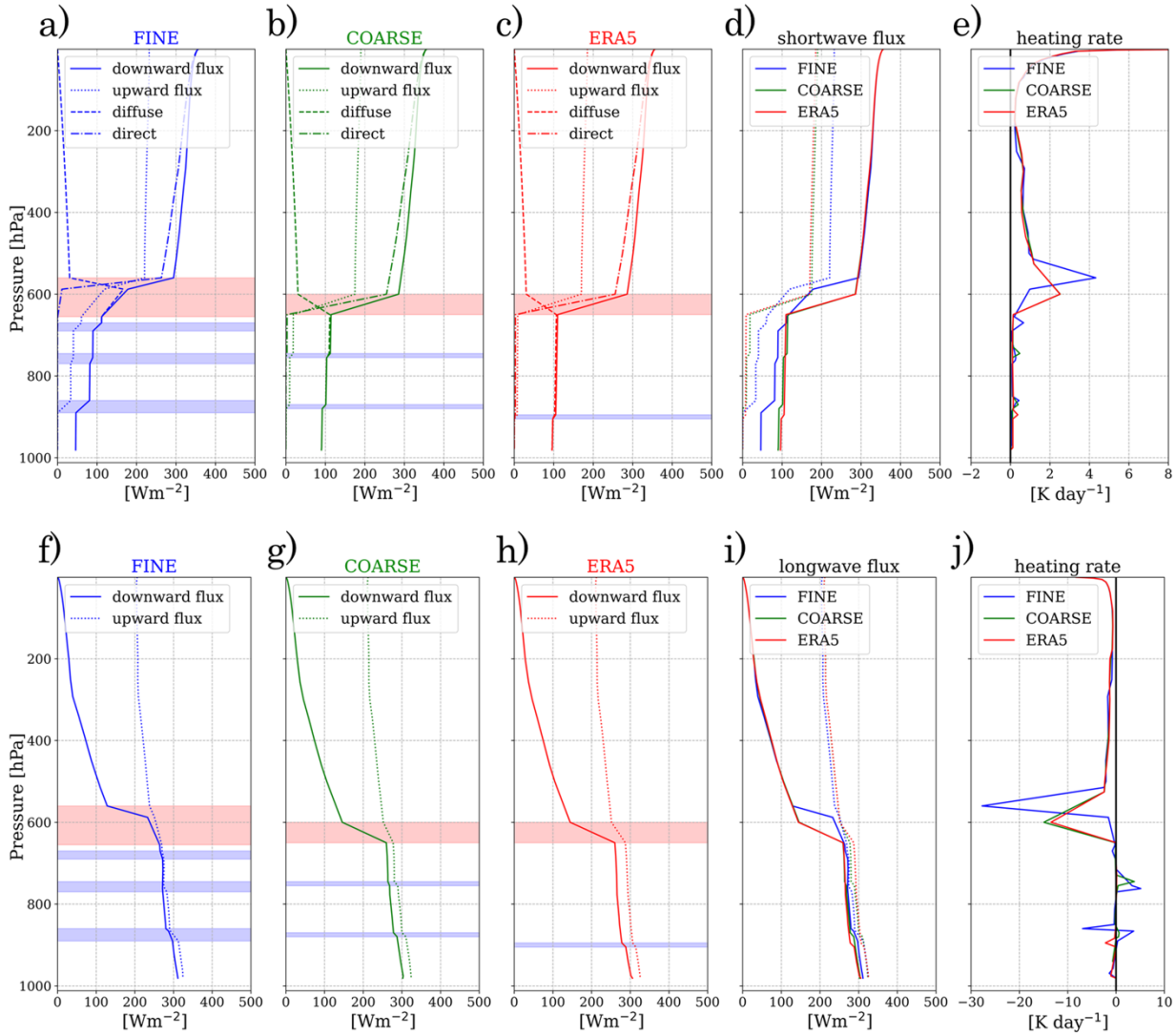

Figure 6. The vertical profiles for 21:56 UTC 15 February 2018 of the SW (a-c)/LW (f-h) downward/upward (solid/dotted lines) and direct/diffuse (dash-dotted/dash) beam flux profiles for the each scenario: a) FINE (blue), b) COARSE (green), and c) ERA5 (red); d,i) the comparison of the SW/LW downward/upward (solid/dotted lines) flux profiles among the four scenarios; e,j) the heating rate profiles due to SW/LW radiative transfer. Positive/negative values represent heating/cooling, respectively.

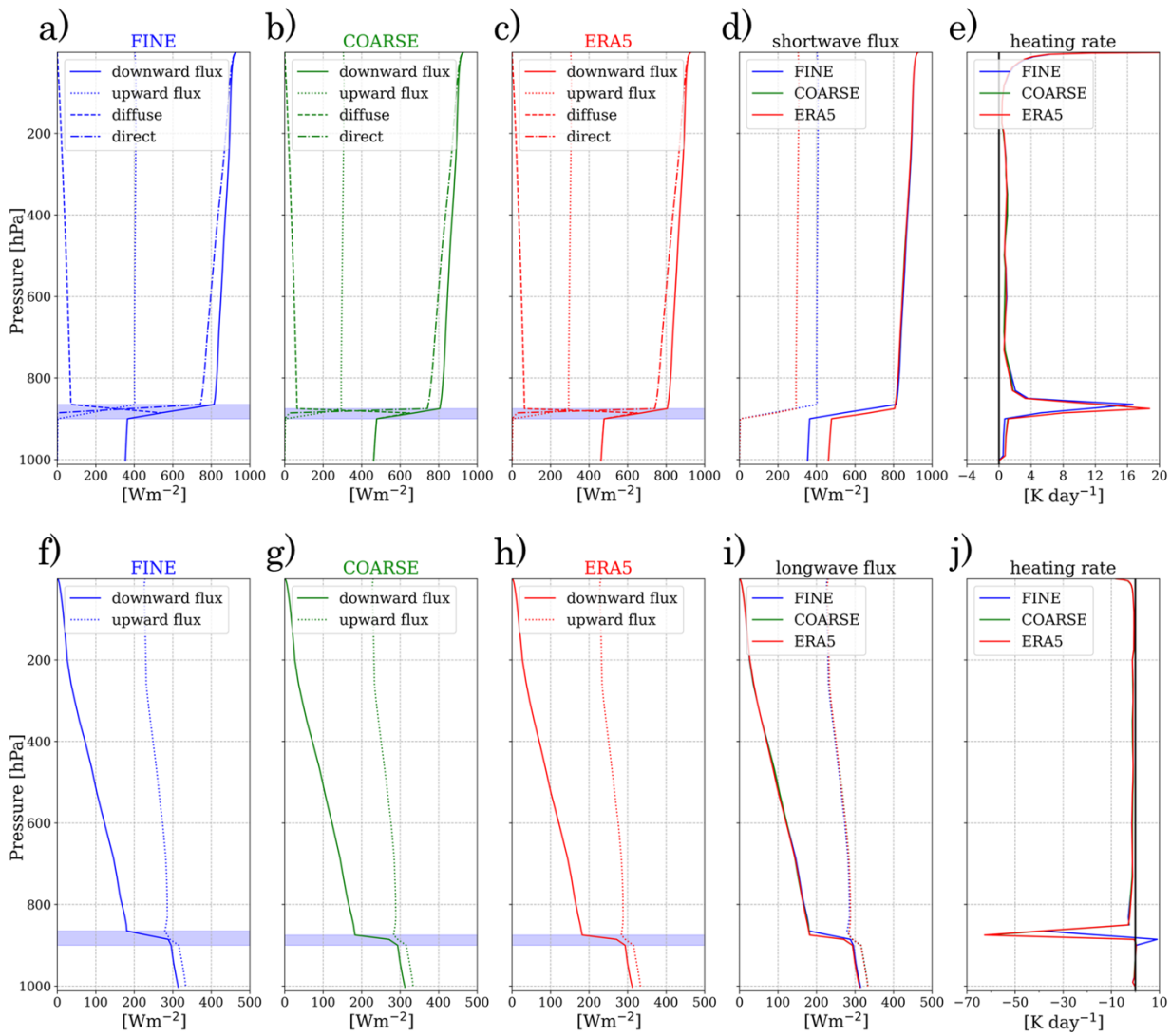

Figure 7. As for Figure 6 but at 04:00 UTC 18 February 2018.

Accepted Article

Accepted Article

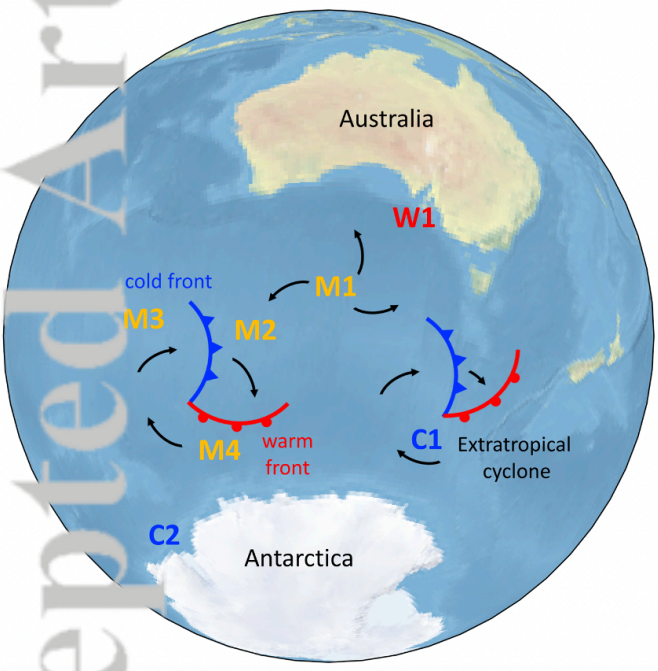

- The ERA5 reanalysis under-represents the number of inferred cloud layers at high latitudes over the Southern Ocean
- Cloud layers inferred from the ERA5 profiles are geometrically thinner and shallower than those inferred from the observed soundings
- A fine-resolution representation of thin multiple cloud layers can help reduce the shortwave radiation bias over the Southern Ocean

JOC_7672_Graphic abstract figure.png